



UNIVERSITY OF LEEDS

This is a repository copy of *Size distribution and solidification of Cu-rich dispersed particles in the core region of stable core shell microstructures of metastable alloy*.

White Rose Research Online URL for this paper:

<https://eprints.whiterose.ac.uk/197453/>

Version: Accepted Version

---

**Article:**

Jegade, OE, Mullis, AM [orcid.org/0000-0002-5215-9959](https://orcid.org/0000-0002-5215-9959) and Cochrane, RF (2023) Size distribution and solidification of Cu-rich dispersed particles in the core region of stable core shell microstructures of metastable alloy. *Journal of Materials Science*, 58 (9). pp. 4213-4222. ISSN 0022-2461

<https://doi.org/10.1007/s10853-023-08287-9>

---

© 2023, The Author(s), under exclusive licence to Springer Science Business Media, LLC, part of Springer Nature. This is an author produced version of an article published in *Journal of Materials Science*. Uploaded in accordance with the publisher's self-archiving policy.

**Reuse**

Items deposited in White Rose Research Online are protected by copyright, with all rights reserved unless indicated otherwise. They may be downloaded and/or printed for private study, or other acts as permitted by national copyright laws. The publisher or other rights holders may allow further reproduction and re-use of the full text version. This is indicated by the licence information on the White Rose Research Online record for the item.

**Takedown**

If you consider content in White Rose Research Online to be in breach of UK law, please notify us by emailing [eprints@whiterose.ac.uk](mailto:eprints@whiterose.ac.uk) including the URL of the record and the reason for the withdrawal request.



[eprints@whiterose.ac.uk](mailto:eprints@whiterose.ac.uk)  
<https://eprints.whiterose.ac.uk/>

# Size distribution and solidification of Cu-rich dispersed particles in the core region of stable core shell microstructures of metastable alloy

*Oluwatoyin E. Jegede, Andrew M. Mullis & Robert F. Cochrane*

School of Chemical & Process Engineering, University of Leeds, Leeds LS2 9JT, UK

## Abstract

The particle size distribution and solidification of dispersed Cu-rich particles within the core region of stable core shell microstructures in drop tube processed metastable Cu-50 at. % Co alloy was studied with a view of understanding the evolution and growth of these microstructures. Microstructural evidence indicates that the formation of the core shell microstructures is highly influenced by nucleation and growth phenomenon. Coalescence propelled by collision is favoured in smaller droplets owing to their higher cooling rates and subsequent higher degree of undercooling to facilitate the liquid phase separation process. Weaker Marangoni motion impeded the further convergence of the Cu-rich particles within the core region.

## Introduction

When immiscible alloys are undercooled into the miscibility gap (MG) which is a dome shaped region on their phase diagrams, separation of the initial homogeneous melt occurs into  $L_1$  and  $L_2$  phases which are of different composition to that of the initial melt [1]. The liquid phase separation (LPS) could either be by nucleation if undercooled into the binodal region or by spinodal decomposition if undercooled into the spinodal region. Undercooling is therefore a pre-requisite for this to occur and large undercooling is only feasible in the absence of heterogeneous nucleation sites [2]. Under terrestrial conditions, these alloys are greatly influenced by gravity resulting in the formation of layered structures with the denser phase occupying the bottom layer [1, 3]. Containerless processing techniques such as drop tube (DT) processing has the combined advantages of rapid solidification at high degrees of undercooling and low gravity conditions thereby eliminating gravity induced effects and less contamination due to the absence of container wall [4]. The phase separation process has been said to start with the nucleation of the liquid minority phase droplets (MPD), growth of the droplets then occurs through the process of diffusion. These droplets have also been known to migrate due to concentration or temperature gradient [1]. The Cu–Co system has a near symmetrical metastable MG below its equilibrium liquidus [5] and when sufficiently undercooled the alloy undergoes metastable liquid phase separation into  $L_1$  (cobalt rich) and  $L_2$  (copper rich) liquid phases [2, 6, 7]. Recently, interest has been on the size distribution pattern of the MPD as this has been said to provide crucial understanding into coarsening process and microstructural evolution behaviour in rapidly solidified immiscible alloys [8].

Potard [9] and Liu et al. [10] studied the Al–In alloy system and observed nano-sized In-rich particles dispersed in Al-rich matrix. Bimodal distribution of the particles was observed with bigger particles said to be dominant at LPS stage while smaller ones are prevalent during monotectic solidification [10]. The prevalence of the larger particles in their research made them conclude that the non-equilibrium solidification of the alloy is dominated by LPS process. Moore et al. [11] and Luo and Chen [12] also observed bimodal size distribution of Pb-rich particles dispersed in Al-rich matrix in the Al-0.7at.% Pb alloy. Moore et al. [11] rapidly solidified the alloy using chill casting and melt spinning and observed nano-sized particles in the melt spun samples and micron sized particles in the chill cast specimens. Using the conclusion from Liu et al. [10], it is reasonable to say that the chill cast samples were at the LPS stage while the melt spun ones had progressed out of the MG and gone beyond the monotectic point. Luo and Chen [12] on the other hand employed electro magnetic

levitation (EML) and then DT in processing the alloy. They observed that dispersed particles in samples processed in EML and then in DT were considerably smaller in size than samples processed via EML alone leading to the conclusion that microgravity had refining effect on dispersed Pb-rich particles.

Liu et al. [10] also observed that cooling rate had significant refining effect on dispersed particles. They noticed refining of In-rich particles in their melt spinning experiment. The size of the MPD increased with increasing distance from the chill surface. Wang et al. [13] and Sun et al. [14] also noticed the refining effect of cooling rate on dispersed Cr-rich particles in melt spun Cu–Cr alloys. Wang et al. [13] in Cu-35 at.% Cr alloy observed nano-sized Cr-rich particles (< 300 nm) which showed evidence of secondary LPS evidenced by the presence of Cu-rich phase in the nodular structures. Sun et al. [14] observed in various Cu–Cr alloys that peak refinement of the Cr-rich particles occurred at cooling rate of magnitude  $106 \text{ Ks}^{-1}$  beyond which LPS was not retained. It was further stated that the size of the dispersed Cr-rich particles was composition dependent as it was observed to increase within the range of 15 to 35 at.% Cr content. The cooling rate effect on dispersed MPD was also highlighted by Fihey et al. [15] in their study on the Cu–Nb alloy system. They suggested from their work on Cu-5 at.% Nb alloy that the size, distribution pattern and shape of the dispersed Nb-rich particles was dependent on the cooling rate.

Undercooling has also been stated to have effect on the size of dispersed particles [16, 17]. The size of dispersed  $L_1$  spheres (Fe-rich) was found to increase with increasing undercooling in the Cu–Fe alloy system and was said to be as a result of accelerated coalescence rate [16]. In gas atomized Cu-15 at.% Fe alloy, He and Zhao [17] found that the size of the dispersed MPD decreased as the parent droplet size decreased but increased in number density. They also observed increased undercooling as the parent droplet size dropped. Using numerical simulation, they established the relationship in Eq. (1) relating the radius ( $r$ ) of the Fe-rich spheres with the diameter ( $D$ ) of the parent droplet.

$$r = 49D^{0.437} \quad (1)$$

There has also been extensive research on dispersed MPD in the Cu–Co system. The selection of phase that is dispersed as the MPD in the Cu–Co system is said to be highly dependent on the critical value of the cobalt phase present which was placed at about 41.6 at.% Co [18]. Co-rich particles are favourably dispersed in a Cu-rich matrix when  $\text{Co} < 41.6 \text{ at. \%}$  while Cu-rich particles disperse in Co-rich matrix when the condition  $\text{Co} > 41.6 \text{ at. \%}$  holds [19].

Cao et al. [18] reported  $L_2$  phase (Cu-rich) dispersed in a Co-rich matrix in drop tube processed Cu-60 wt.% Co alloy. They observed that the dispersed particles were finer in the smaller droplets (diameter range of 0.2 to 2.2  $\mu\text{m}$ ) and their number density much larger than in the bigger droplets whose diameter ranged from 0.6 to 5.0  $\mu\text{m}$ . Particle size in a 400  $\mu\text{m}$  droplet was between 0.6 and 1.6  $\mu\text{m}$ . The refinement and the significant increase in the number density of the particles in the smaller droplet size was attributed to the cooling rate which was found to increase drastically as the droplet size decreased; this in turn is said to result in increased undercooling and ultimately propagation of LPS by nucleation and growth. This is also supported by the findings of Zhao et al. [20] that at higher cooling rates, the density of nuclei are considerably higher. Higher undercooling in the smaller droplets is said to be due to the lower probability of impurities in them compared to the larger droplets [18].

Kolbe and Gao [21] used both EML and 8 m drop tube to process the Cu-16 at.% Co alloy and the dispersed phase was different to that observed by Cao et al. [18].  $L_1$  phase (Co-rich) dispersed in Cu-rich matrix in both experiments. Generally, the average radii of particles dispersed in the EML samples were larger (in  $\mu\text{m}$ ) than in the drop tube samples owing to increased convection during the

EML process which lead to the collision and coagulation of the particles. Bimodal size distribution of particles was observed in the EML processed droplets with the peak at small size said to indicate normal growth behaviour while that at large size signifies influence of convection. However, particles in the drop tube samples in the sieve size range 224 to 280  $\mu\text{m}$  were found to be in two major categories: those with average radius of 220 nm and those with average radius range of 300 to 790 nm.

Various studies on dispersed particles in Cu–Co alloys using EML have also been done by Zhang et al. [8, 19, 22, 23]. In Cu-50 at.% Co alloy they found that in the absence of magnetic field, bimodal size distribution of dispersed Cu-rich particles obtains while in the contrary single distribution pattern was observed [22]. Bimodal size distribution of particles was also observed in the Cu-25 at.% Co alloy when the magnetic field is increased marginally up to a value of 0.5 T beyond which single distribution pattern is obtained [19]. The singular distribution pattern is similar to what was observed by Kolbe and Gao [21] in drop tube samples and is attributed to reduced coagulation of the particles due to reduced convection in drop tubes [19]. A comparison of the bimodal distribution of dispersed Co-rich particles in the Cu-25at.% Co and Cu-16 at.% Co alloys was also carried out by Zhang et al. [23]. They found that the size distribution as well as composition variation of the dispersed particles became broader with increased cobalt content of the alloy. In the ternary alloy Cu–Co–Ni, they observed a change in the size distribution pattern from bimodal to multi modal as the undercooling increased [8].

All these studies reasonably undercooled the Cu–Co alloys enough to get it to liquid phase separate evidenced by the dispersed spherical particles. However, there is tendency that when immiscible alloys are processed in microgravity environment such as is obtained in a drop tube; a thermal gradient is induced inside the falling droplet. This thermal gradient leads to the Marangoni motion of particles towards the region of higher temperature which in this case is the centre of the droplet. However, evidence of Marangoni motion of the particles were not reported in these studies on the Cu–Co alloy system. The Marangoni convection leads to the formation of core shell microstructures which has only been reported in drop tube processed Cu–Co alloys by Jegede et al. [24]. They reported the presence of Cu-rich particles dispersed in the bulk Co-rich core and concluded this was indicative of the occurrence of two simultaneous liquid phase separation events.

This paper therefore builds on the previous study of Jegede et al. [24] mentioned above and seeks to provide novel insight into the distribution of dispersed Cu-rich particles and the subsequent impact on the solidification process of the core shell microstructures in the Cu-50 at.% Co alloy. The effect of droplet size variation and undercooling on the particle size distribution in these structures are also examined.

### Experimental methods

Bulk samples of the Cu–Co alloy is prepared by alloying pure Cu (99.999%) and Co (99.99%) in an electric arc furnace under an argon environment. In order to ensure complete mixing of the elemental components, the arc melting process was done nine times with the sample being flipped over between each melting cycle. The drop tube processing was done by placing slices from the produced arc melt ingot into the crucible of a 6.5 m drop tube. The crucible assembly was placed in a graphite susceptor encased in an aluminium shield surrounded by induction coils at the top of the drop tube. Prior to melting, the drop tube was purged three times by evacuating the system and refilling with nitrogen. The last evacuation was to a pressure of 10–4 Pa and backfilled with nitrogen gas to 40 kPa. The crucible was inductively heated and the melted alloy in it was superheated to 200 K above its equilibrium liquidus. The superheated melt was then ejected under pressure into the drop tube through the holes at the base of the crucible thereby forcing the melt to disperse into varying sized droplets which rapidly solidified during their free fall down the tube.

The cooled rapidly solidified drop tube powders at the base of the tube were collected and then sorted into standard wire mesh sieve sizes. The different sieve sized droplets were subjected to metallographic procedure by hot mounting in transoptic resin and subsequent grinding and polishing to expose their surfaces. Etching with nital solution (2% nitric acid and 98% propan-2-ol) was done so as to have better contrast of the regions within the droplets. Detailed experimental setup and full description of the metallographic procedure of the alloy considered in this article is available in an earlier publication [24]. Microstructures were examined using a BX51 Olympus optical microscope fitted with a Zeiss AxioCam™ MRc5 camera and a Carl Zeiss Evo MA 15 scanning electron microscope (SEM) equipped with energy dispersive X-ray spectrometer (EDS). Backscattered electron imaging (BSE) mode was employed. Subsequent size distribution of phases present in the droplets was determined by stereo metallographic method using imageJ software.

## Results

The morphology of the microstructure observed in the drop tube powders are of two types: The first type which exhibited no signs of liquid phase separation is tagged NLPSS (non-liquid phase separated structures) and consists of fragmented and non-fragmented dendrites. The second variant showing signs of liquid phase separation are tagged LPSS (liquid phase separated structures) and consists of stable core shell structures (SCSS) and evolving core shell structures (ECSS) which are non-spherical structures at different stages along the coalescence process, but clearly have distinct regions. The stable core shell structures on the other hand have clearly defined spherical core with concentric shell regions unlike the other LPSS described in [24]. Using imageJ, a count of each of the type of structure in the different sieve size fractions was taken and Fig. 1a shows the frequency distribution of the NLPSS to the LPSS per sieve size fraction of the drop tube powders. It is seen that the LPSS are prevalent in the smaller size fractions owing to likelihood of higher degree of undercooling in the smaller droplets as a result of their higher cooling rates. An estimate of the cooling rate as a function of droplet size in drop tube processed Cu-50 at. % Co alloy has been shown to be approximated by the power relation  $(1.815 \times 10^7) (d/\mu\text{m})^{-1.476}$  [24] and Fig. 1b shows the cooling rate variation in the alloy with a droplet of 38  $\mu\text{m}$  having an estimated cooling rate of  $8.02 \times 10^4 \text{ Ks}^{-1}$  compared to  $8.39 \times 10^2 \text{ Ks}^{-1}$  in a much larger droplet of diameter 850  $\mu\text{m}$ .

The fully evolved stable core shell structures (SCSS) is the only structure of the LPSS category considered in this study and its morphology as revealed by Z—contrast in backscattered image mode consists of dark particles in a lighter matrix. Colour contrast and EDS measurements confirms dark particles are Co-rich dispersions in a lighter Cu-rich matrix. Figure 2a and b shows the typical SCSS of the Cu-50 at. % Co alloy solidified during free fall in a drop tube. They are characterised by a darker Co-rich core at the centre of the droplet encased by a lighter Cu-rich shell. Both the core and shell contained inclusions. The shell contained dispersion of Co-rich spherical particles or dendrites and in some instances both types of inclusion are simultaneously present while the core either contained a dispersion of Cu-rich spherical particles or loop-like structure which contain very fine scale Cu-rich particles (Fig. 2a). The pattern of the dispersed phase in this study is in tandem with the results of Kolbe and Gao [21] but contrary to the observation in the drop tube studies of Cao et al. [18] and Zhao et al. [20]. Also, the assertion by Zhang et al. [19] that the Cu-rich phase is favourably dispersed when the content of Co > 41.6% is invalidated in this present study.

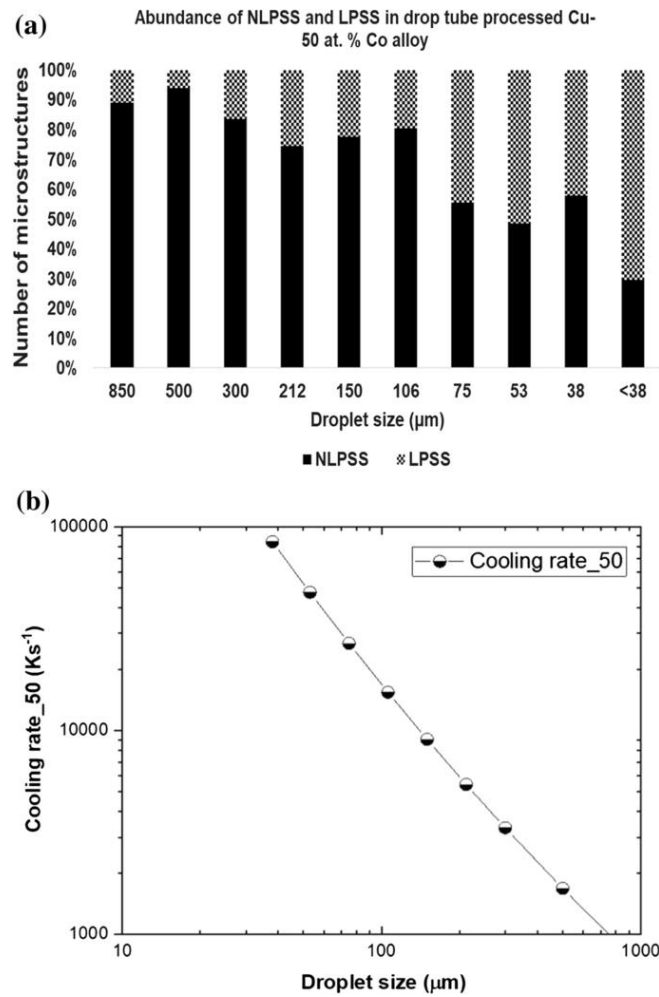


**Figure 1 a** Distribution of non-liquid phase separated structures (NLPSS) and liquid phase separated structures (LPSS) with droplet diameter in drop tube processed Cu-50 at. % Co alloy. **b** Cooling rate variation with droplet size in drop tube processed metastable Cu-50 at. % Co alloy

The size distribution of the dispersed Cu-rich particles within the core of the SCSS is carried out as this could give an insight into the evolution and growth of these structures. The frequency distribution of the apparent radius of the dispersed particles normalised with respect to the overall particle population in five consecutive size fractions with significant population of stable core shell microstructures is shown in Fig. 3.

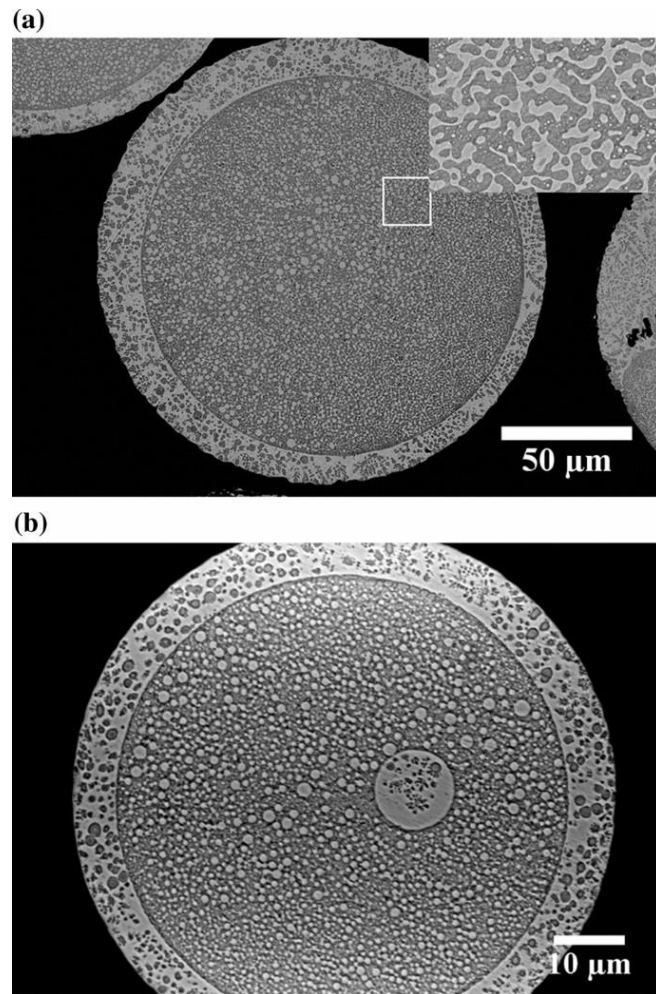


**Figure 2** **a** Stable core shell showing core region characterized by loop-like structure with fine scale Cu-rich particles (enlarged part). **b** Stable core shell microstructure with Co-rich particles in the shell and Cu-rich particles dispersed in the core region.

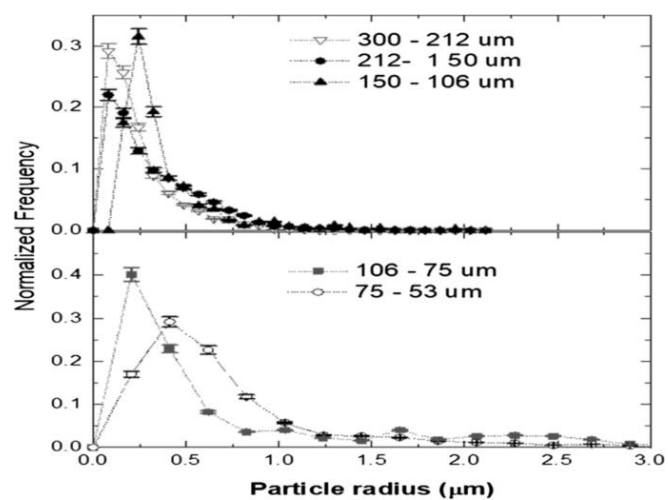


**Figure 3.** Normalized frequency of particle size distribution of Cu-rich particles within the core of stable core shell microstructure as a function of particle radius in different sized droplets of drop tube processed Cu-50 at.% Co alloy.

In the larger droplets (300–212  $\mu\text{m}$  size range), majority of the dispersed Cu-rich particles had diameter of 0.15  $\mu\text{m}$ . However, as the size fraction of the droplets decreased, the dispersed particles became smaller with most of the particles having diameter of 0.04  $\mu\text{m}$  an exception being the 150–106  $\mu\text{m}$  size range in which the observed diameter of the Cu-rich particles were majorly 0.07  $\mu\text{m}$ . The mean particle size in three size fractions (300–212, 212–150 and 75–53  $\mu\text{m}$ ) was 0.4  $\mu\text{m}$  while in the 150–106  $\mu\text{m}$  and 106–75  $\mu\text{m}$  droplets, the average particle size recorded was 0.15  $\mu\text{m}$  and 1.25  $\mu\text{m}$ , respectively. The observed results is consistent with similar drop tube studies on the alloy system in that a refining effect in the size of the dispersed particles is observed as the parent droplet size reduced and this is largely attributed to the variance of the cooling rate in the droplets [18, 20].

### Discussions

As the falling droplet accesses deeper undercooling, its temperature falls within the binodal region and a primary LPS process is initiated with the nucleation of Co-rich spherical particles which under the forces of collision coalesces to form larger particles. Thermal gradient induced in the falling droplet causes Marangoni motion of the coalesced particles towards the center of the droplet thereby forming the distinct Co-rich core and Cu-rich shell and concluding the primary LPS process. Two events are however likely as the solidification process proceeds: the first is that with higher cooling rates, the temperature drops below the spinodal region and a secondary LPS process is initiated. Due to different parts of the droplet having different compositions, the artefacts of this secondary LPS process in the different parts of the droplet will vary. This explains the occurrence of SCSS with spinodally decomposed core as shown in Fig. 2a. The second occurrence is in the event of the temperature of the solidification process remaining within the binodal region and due to the composition of the distinct core and shell, a second LPS process after the manner of the primary LPS process occurs. This second LPS process is thought to be the route of core shell structures similar to that shown in Fig. 2b. The structures that have undergone this route have shells possessing Co-rich spherical particles with or without fine scale Cu-rich dispersions and cores with dispersed Cu-rich particles.

The observed normal singular distribution pattern with extensive tail of the Cu-rich particles within the core has been attributed to minimal coagulation of dispersed particles as a result of reduced convection during drop tube processing [19, 21, 22]. Despite the higher cooling rate in smaller droplets (as shown in Fig. 1b), the distribution pattern appears uniform irrespective of the size fraction indicative of minimal effect of cooling rate on the distribution pattern contrary to the observations of Fihey et al. [15]. However, the refinement of the diameter of most of the dispersed particles as the droplet size decreased is attributed to the increased cooling rate and subsequently increased undercooling in the smaller droplets [18, 20]. As the degree of undercooling gets higher, the nucleation rate increases hence abundance of smaller dispersed particles than in the larger droplet sizes. On the other hand, the increased nucleation also means increased population and as such propensity for coagulation of the dispersed particles implying that liquid phase separation in the alloy system is heavily characterised by nucleation and growth phenomenon. The nucleation and growth hypothesis could explain the large Cu-rich particle observed in Fig. 2b. Table 1 shows the diameter of the largest particle in each of the size fraction:

**Table 1** Diameter of largest Cu-rich particle within the core of various core shell microstructures

Droplet size range ( $\mu\text{m}$ )	Diameter of largest dispersed Cu-rich particle ( $\mu\text{m}$ )
300–212	4.2
212–150	3.3
150–106	1.0
106–75	10.4
75–53	3.2

Relating these to the general abundance of core shell microstructures as shown in Fig. 1a, seems to suggest when conditions are such that more NLPSS are available, the solidification of the core shell microstructures terminate at the secondary liquid phase separation stage leading to the formation of the L2 dispersed Cu-rich particles in the core of the stable core shell microstructures. However, when conditions are such that there are equal abundance of NLPSS and LPSS (106–75  $\mu\text{m}$  size fraction), increased particle movement is favoured. Microstructural evidence in this research suggests that at this condition, coagulation of the L2 Cu-rich particles into larger ones occurred and as such further liquid phase separation into L3 Co-rich particles (as seen in Fig. 2b) or Co-rich dendrites were formed (shown in Fig. 4). It is probable that if these core shell microstructures were not frozen at the stage at which they were captured, an onion-like core shell microstructure [24] could have been formed. However, no onions-like microstructures were observed in this research.

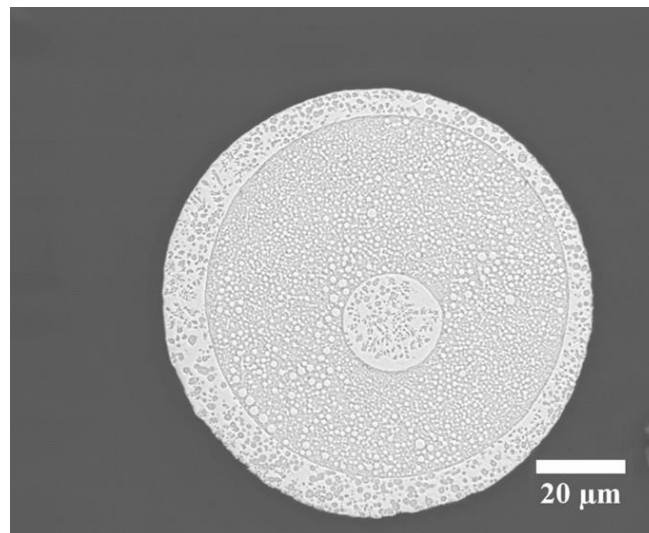


**Figure 4.** Stable core shell microstructure showing a large Cu-rich particle with dendrites within its core.

Due to the continuous enrichment of the center of the parent droplet with the Co-rich phase to form the core, the shell becomes depleted of this phase and as a result a concentration gradient is created between the core and shell regions. This concentration gradient induces solutal Marangoni effect which drives particles outward in opposite direction to the thermal Marangoni motion. The overall Marangoni direction then depends on the greater of the two.

Certainly, thermal Marangoni was effective in the parent droplet despite the obvious difference in the concentration of the core and shell region. However, the presence of the L<sub>2</sub> (Cu-rich) particles within the core necessitates the concentration profile of the core be taken to ascertain whether solutal Marangoni was responsible for their movement since they have been shown capable of further growth. The concentration profile of series of concentric circles of the core region in two sieve size fractions (212–150 μm and 106–75 μm) was taken (Fig. 5a). The EDX result (Fig. 5b) showed that the cobalt concentration of the core was fairly constant implying that another mechanism was responsible for the L<sub>2</sub> particles movement within the core region.

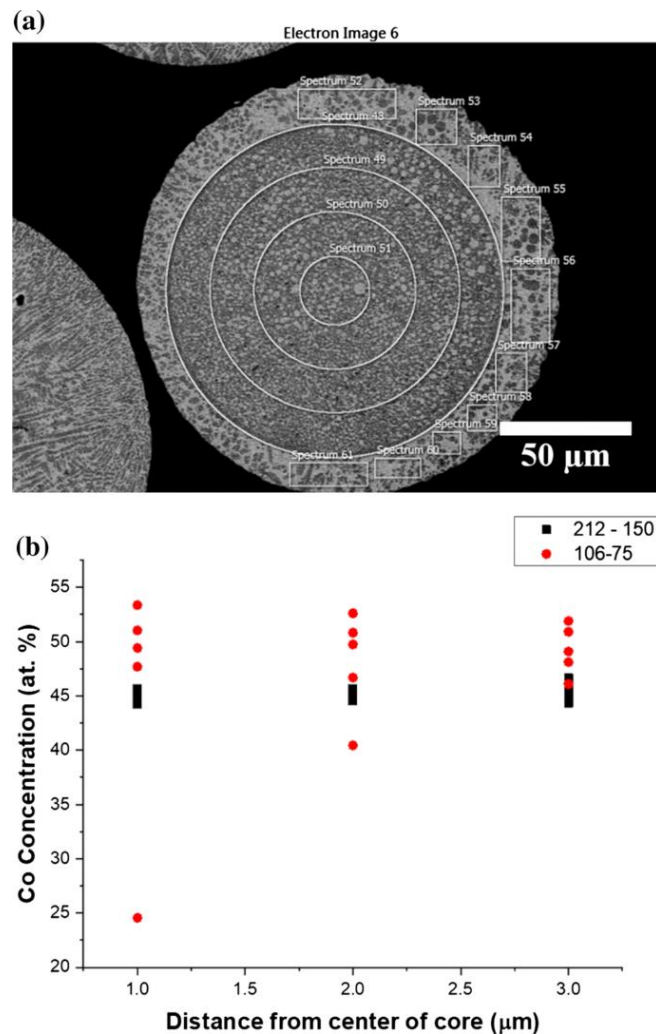


**Figure 5a** EDX profile of the concentration within the core region of a core shell structure with increasing distance from the centre. **b** EDX result for cobalt concentration within the core region of a core shell structure with increasing distance from the centre in two sieve size fractions.

### Summary and conclusion

Generally, in order for SCSS to form, the parent droplet are undercooled into the miscibility gap and nucleation of Co-rich particles are initiated at the surface in contact with the inert gas of the drop tube. In a bid to reduce energy of the system, the Co-rich particles coalesce by collision to form larger ones and these are driven towards the center of the parent droplet by Marangoni motion as a result of existing thermal gradient leading to the formation of Co-rich core thereby concluding a primary liquid phase separation process. Within the core, liquid phase separation is also initiated with the nucleation of Cu-rich particles. In a bid to also reduce energy, the nucleated Cu-rich particles also coalesce by collision to form larger particles. However, as earlier explained the coalescence is favoured in smaller

droplets specifically in the size fraction which favours equal number of LPSS and NLPSS (106–75  $\mu\text{m}$ ). Hypothetically, stronger Marangoni motion would ensure the convergence of the  $L_2$  Cu-rich particles at the centre of the core but this was not the case. Further liquid phase separation occurred within the dispersed  $L_2$  Cu-rich particles into Co-rich particles / dendrites. Without sufficient undercooling into the metastable miscibility gap, liquid phase separation and subsequent formation of core shell structures is not feasible.

## References

1. Zhou ZM, Gao J, Li F, Zhang YK, Wang YP, Kolbe M (2009) On the metastable miscibility gap in liquid Cu–Cr alloys. *J Mater Sci* 44:3793–3799. <https://doi.org/10.1007/s10853-009-3511-y>
2. Munitz A, Abbaschian R (1996) Microstructure of Cu–Co alloys solidified at various supercoolings. *Metall Mater Trans A* 27:4049–4059. <https://doi.org/10.1007/BF02595654>
3. Ratke L, Korekt G, Brück S, Schmidt-Hohagen F, Kasperovich G, Köhler M (2009) Phase equilibria and phase separation processes in immiscible alloys, in: 2nd Sino Ger Symp
4. Herlach DM, Holland-Moritz D, Galenko P (2006) *Metastable solids from undercooled melts*, Elsevier
5. Nakagawa Y (1958) Liquid immiscibility in copper-iron and copper-cobalt systems in the supercooled state. *Acta Metall* 6:704–711. [https://doi.org/10.1016/0001-6160\(58\)90061-0](https://doi.org/10.1016/0001-6160(58)90061-0)
6. Yamauchi IN, Ueno M, Shimaoka IO (1998) Undercooling in Co—Cu alloys and its effect on solidification structure. *J Mater Sci* 33:371–378. <https://doi.org/10.1023/A:1004319829612>
7. Munitz A, Abbaschian R (1991) Two-melt separation in supercooled Cu–Co alloys solidifying in a drop-tube. *J Mater Sci* 26:6458–6466. <https://doi.org/10.1007/BF00551897>
8. Zhang Y, Wu Z, Wang M, Yang C, Wilde G (2014) Effect of undercooling on particle size distribution in phase separated Cu<sub>75</sub>Co<sub>25</sub>-xM<sub>x</sub> (M = Ni, Fe) alloys with low M content. *J Alloys Compd* 596:55–57. <https://doi.org/10.1016/j.jallcom.2014.01.182>
9. Potard C (1982) Structures of immiscible Al–In alloys solidified under microgravity conditions. *Acta Astronaut* 9:245–254. [https://doi.org/10.1016/0094-5765\(82\)90027-3](https://doi.org/10.1016/0094-5765(82)90027-3)
10. Liu Y, Guo J, Su Y, Ding H, Jia J (2001) Microstructure of rapidly solidified Al–In immiscible alloy. *Trans Nonferrous Met Soc China* 11:84–89
11. Moore K, Zhang D, Cantor B (1990) Solidification of Pb particles embedded in Al. *Acta Metall Mater* 38:1327–1342. [https://doi.org/10.1016/0956-7151\(90\)90205-U](https://doi.org/10.1016/0956-7151(90)90205-U)
12. Luo X, Chen L (2008) Investigation of microgravity effect on solidification of medium-low-melting-point alloy by drop tube experiment. *Sci China Ser E Technol Sci* 51:1370–1379. <https://doi.org/10.1007/s11431-008-0128-3>
13. Wang Y, Song X, Sun Z, Zhou X, Guo J (2007) The solidification of CuCr alloys under various cooling rates. *Mater Sci Pol* 25:199–207
14. Sun Z, Wang Y, Guo J (2006) Liquid phase separation of Cu–Cr alloys during rapid cooling. *Trans Nonferrous Met Soc China* 16:998–1002. [https://doi.org/10.1016/S1003-6326\(06\)60367-1](https://doi.org/10.1016/S1003-6326(06)60367-1)
15. Fihey JL, Nguyen-Duy P, Roberge R (1976) On the solidification microstructure of copper-rich niobium alloys. *J Mater Sci* 11:2307–2311. <https://doi.org/10.1007/BF00752095>
16. Chen YZ, Liu F, Yang GC, Xu XQ, Zhou YH (2007) Rapid solidification of bulk undercooled hypoperitectic Fe–Cu alloy. *J Alloys Compd* 427:L1–L5. <https://doi.org/10.1016/J.JALLCOM.2006.03.012>
17. He J, Zhao J (2005) Behavior of Fe-rich phase during rapid solidification of Cu–Fe hypoperitectic alloy. *Mater Sci Eng A* 404:85–90. <https://doi.org/10.1016/J.MSEA.2005.05.045>
18. Cao CD, Wei B, Herlach DM (2002) Disperse structures of undercooled Co-40 wt% Cu droplets processed in drop tube. *J Mater Sci Lett* 21:341–343. <https://doi.org/10.1023/A:1017913029777>
19. Zhang Y, Gao J, Yasuda H, Kolbe M, Wilde G (2014) Particle size distribution and composition in phase-separated Cu<sub>75</sub>Co<sub>25</sub> alloys under various magnetic fields. *Scr Mater* 82:5–8. <https://doi.org/10.1016/j.scriptamat.2014.03.003>

20. Zhao JZ, Ratke L, Feuerbacher B (1998) Microstructure evolution of immiscible alloys during cooling through the miscibility gap. *Model Simul Mater Sci Eng* 6:123–139
21. Kolbe M, Gao JR (2005) Liquid phase separation of Co-Cu alloys in the metastable miscibility gap. *Mater Sci Eng A* 413–414:509–513. <https://doi.org/10.1016/j.msea.2005.08.170>
22. Zhang YK, Gao J, Nagamatsu D, Fukuda T, Yasuda H, Kolbe M, He JC (2008) Reduced droplet coarsening in electromagnetically levitated and phase-separated Cu-Co alloys by imposition of a static magnetic field. *Scr Mater* 59:1002–1005. <https://doi.org/10.1016/j.scriptamat.2008.07.005>
23. Zhang Y, Gao J, Wei L, Kolbe M, Volkmann T, Herlach D (2011) Novel insight into microstructural evolution of phase-separated Cu–Co alloys under influence of forced convection. *J Mater Sci* 46:6603–6608
24. Jegede OE, Cochrane RF, Mullis AM (2018) Metastable monotectic phase separation in Co–Cu alloys. *J Mater Sci* 53:11749–11764. <https://doi.org/10.1007/s10853-018-2417-y>